Published in final edited form as:
Mol Pharm. 2014 January 6; 11(1): 40–48. doi:10.1021/mp4005244.

Ultrasound-Mediated Destruction of LHRHa Targeted and Paclitaxel Loaded Lipid Microbubbles Induces Proliferation Inhibition and Apoptosis in Ovarian Cancer Cells

Hongxia Liu[†,#], **Shufang Chang**[†,*], **Jiangchuan Sun**[†,#], **Shenyin Zhu**[ξ,#], **Caixiu Pu**[†], **Yi Zhu**[†], **Zhigang Wang**[‡], and **Ronald X. Xu**[†,§]

[†]Department of Obstetrics and Gynecology, Second Affiliated Hospital of Chongqing Medical University, Chongqing 400010, China

[‡]Institute of Ultrasound Imaging, Second Affiliated Hospital of Chongqing Medical University, Chongqing 400010, China

[ξ]Department of Pharmacy, First Affiliated Hospital of Chongqing Medical University, Chongqing 400016, China

[§]Department of Biomedical Engineering, The Ohio State University, Columbus, OH 43210, USA

Abstract

Although paclitaxel (PTX) is used with platinum as the first line chemotherapy regimen for ovarian cancer, its clinical efficacy is often limited by severe adverse effects. Ultrasound targeted microbubble destruction (UTMD) technique holds a great promise in minimizing the side effects and maximizing the therapeutic efficacy. However, the technique typically uses non-targeted microbubbles with suboptimal efficiency. We synthesized targeted and PTX-loaded microbubbles (MBs) for UTMD mediated chemotherapy in ovarian cancer cells. PTX-loaded lipid MBs were coated with a luteinizing hormone-releasing hormone analogue (LHRHa) through a biotin-avidin linkage to target the ovarian cancer A2780/DDP cells that express the LHRH receptor. In the cell culture studies, PTX-loaded and LHRHa targeted MBs (TPLMBs) in combination with ultrasound (300 kHz, 0.5 W/cm^2, 30 seconds) demonstrated anti-proliferative activities of 41.30 ± 3.93%, 67.76 ± 2.45%, and 75.93 ± 2.81% at 24 hours, 48 hours, and 72 hours after the treatment, respectively. The cell apoptosis ratio at 24 hours after the treatment is 32.6 ± 0.79 %, which is significantly higher than other treatment groups such as PTX only and no-targeted PTX-loaded MBs (NPLMBs) with or without ultrasound mediation. Our experiment verifies the hypothesis that ultrasound mediation of ovarian cancer targeted and drug loaded MBs will enhance the PTX therapeutic efficiency.

Keywords

Paclitaxel; ultrasound; microbubble; ovarian cancer; apoptosis

INTRODUCTION

Ovarian cancer is the fifth leading cause of cancer death in women.[1] Patients commonly develop ovarian cancer asymptomatically and present with peritoneal metastasis at the time

[*]Corresponding author. Mailing address: Department of Obstetrics and Gynecology, Second Affiliated Hospital of Chongqing Medical University, No.74 Linjiang Road, Yuzhong district, Chongqing 400010, China. Tel.: +86 23 6369 3729; fax: +86 23 65104238. shfch2005@163.com (S. Chang).
[#]These authors contributed equally to this work.

of diagnosis.[2] Although primary and large tumor nodules may be removed by cytoreductive surgery, micronodular and floating tumor colonies cannot be removed surgically. Therefore, extensive chemotherapy is necessary. Today, paclitaxel (PTX) and platinum are the first line chemotherapy regimens commonly used for treating ovarian cancer.[3] They have several limitations such as severe bone marrow depression and peripheral neuropathy.[4–7] Therefore, the combination of targeted delivery and controlled release of chemotherapies holds a great promise in minimizing the side effects and maximizing the therapeutic efficacy.[8,9]

In the past decades, great efforts have been made on engineering specialized delivery systems that encapsulate chemotherapeutic drugs for controlled and sustained release. These drug delivery carriers include biodegradable polymers, water-soluble prodrugs, microemulsions, nanoparticles, and liposomes. The ultrasound-targeted microbubble destruction (UTMD) technique has exhibited a great potential for drug delivery to solid tumor.[10,11] Microbubbles (MBs) in combination with ultrasound is able to stimulate the permeabilization of cell membranes and increase the drug uptake by tumor cells.[12–14] Ultrasound mediated destruction of PTX loaded MBs for treating solid tumors have been reported by many researchers.[15–18] Previous studies typically focus on non-targeted microbubbles that are readily aggregated in the reticuloendothelial system, leading to a low concentration at the tumor site. In order to improve the therapeutic efficacy and reduce the systemic toxicity, it is necessary to target drug loaded MBs to tumor-specific ligands such as antigens and peptides. Recently, ultrasound mediated destruction of LyP-1 targeted and PTX-loaded MBs have been used for treating breast cancer cells.[19] We have also synthesized a luteinizing hormone-releasing hormone analogue (LHRHa) conjugated MB agent for ultrasound mediated transfection of wild type P53 gene that induced the apoptosis in ovarian cancer cells.[20]

In this study, we coupled the LHRHa ligands with PTX-loaded MBs to target human ovarian cancer A2780/DDP cells that express the LHRH receptor. The PTX loading rate in MBs was characterized by an HPLC system. The LHRHa concentration in MBs was detected by flow cytometry. The binding of MBs to the cancer cells was observed by bright field microscopy. After UTMD mediated delivery of PTX to the cancer cells, the cell apoptosis and the cell cycle were analyzed by flow cytometry. The expression of Caspase-3 and CyclinB1 protein after treatment were evaluated by Western Blot tests. The ultrastructure of A2780/DDP cells was characterized by transmission electron microscopy (TEM). Our experiment verifies the hypothesis that ultrasound mediation of ovarian cancer targeted and drug loaded MBs will enhance the efficacy of PTX therapy. To the best of the author's knowledge, using drug loaded and tumor targeted MBs for UTDM mediated drug delivery to ovarian cancer cells has not reported elsewhere.

Experimental Section

Cell lines and cell cultures

Human ovarian carcinoma A2780/DDP cell lines were a generous gift from Professor Zehua Wang at Wuhan Union Hospital (Wuhan, China). The cells were grown in a HyClone RPMI 1640 medium (Fisher Scientific, Shanghai, China) at 37°C in a humidified incubator containing 5% CO_2, supplemented with 10% heat-inactivated fetal bovine serum (FBS, GIBCO), 100 μg/ml streptomycin and 100 U/ml penicillin (GIBCO). Exponentially growing cells were used for all the experiment.

Preparation of PTX-loaded MBs (NPLMBs)

NPLMBs were fabricated by a modified emulsification process.[21] Five milligrams of 1,2-dipalmitoyl-sn-glycero-3-phosphatidylcholine (Avanti Polar Lipids Inc., Alabaster, AL, USA), two milligrams of 1,2-distearoyl-sn-glycero-3-phosphatidyl-ethanolamine (Avanti),

and two milligrams of PTX (Chengdu Yuancheng Biotechnology Ltd. Co., Chengdu, China) were dissolved in a 1.5 ml vial containing 50 μl of 100 % glycerine and 450 μl of phosphate buffered saline (PBS). The vial was incubated in 40 °C water for 30 minutes. After that, the container was degassed and reperfused with perfluoropropane gas (C_3F_8, MW 188 g/mol, Tianjin Institute of Physical and Chemical Engineering, Tianjin, China). The mixture was then mechanically vibrated for 45 seconds in a dental amalgamator (YJT Medical Apparatuses and Instruments, Shanghai, China) at a vibration frequency of 60 Hz. The resultant white mixture was diluted with PBS to obtain the non-targeted and PTX-loaded lipid MBs (NPLMBs).

Preparation of LHRHa-targeting PTX-loaded MBs (TPLMBs)

TPLMBs were fabricated by a modified emulsification process.[19, 20] The process consisting of three consecutive steps: (1) biotinylating PTX-loaded MBs to obtain BPLMBs, (2) avidinylating BPLMBs to obtain BSPLMBs, and (3) conjugating BSPLMBs with biotinylated LHRHa peptide to obtain TPLMBs. The experimental details for each step are described below. BPLMBs were prepared by replacing 1,2-distearoyl-sn-glycero-3-phosphatidyl-ethanolamine with 1,2-distearoyl-sn- glycero-3-phosphatidyl-ethanolamine-N-[Biotinyl (Polye thylene Glycol) 2000] (Avanti) in the above recipe. The prepared BPLMBs were then washed with PBS solution three times in a bucket rotor centrifuge at 800 g for three minutes to remove the excess unincorporated lipids from the MBs. After that, 50 μg of streptavidin (SA, Beijing Biosynthesis Biotechnology Co., Ltd., China) per 10^8 MBs was added to the washed MB dispersion. The MBs were then incubated at 4°C for 20 minutes, washed three times at the same centrifugation condition to remove unreacted streptavidin and obtain BSPLMBs, and incubated at 4 °C with 50 μg of biotinylated LHRHa peptides (with amino acid sequence: pGlu-His-Trp-Ser-Tyr-D-leu-leu-Arg-Pro-NH_2, synthesized by Beijing SciLight Biotechnology Co. Ltd., Beijing, China) per 10^8 MBs for another 20 minutes. The mixture was then washed with PBS to remove free ligands and obtain TPLMBs. NPLMBs, BNPLMBs and TPLMBs were sterilized by cobalt 60 (^{60}Co) irradiation. Fluorescent MBs were prepared according to the same protocol except that the fluorescent dye DiI (Beyotime Institute of Biotechnology, Jiangsu, China) was added into the lipid mixture during the water bath.

Characterization of TPLMBs

TPLMBs were dispersed in PBS buffer for morphology characterization by a bright field microscope, concentration detection by a blood cell count plate, and size and zeta potential measurement by a Malvern Zetasizer Nano ZS unit (Malvern Instrument, UK). The PTX loading rate was characterized by an Agilent 1100 HPLC system with a Hypersil GOLD C_{18} column (4.6 mm × 250 mm, 5 μm) and a mobile phase of methanol and PBS mixed at the volume ratio of 70:30. The flow rate was set at 1.0 ml/min and the analysis wavelength was at 228 nm. The standard calibration curve derived from the test showed high linearity, accuracy, and reproducibility, with a correlation coefficient of 0.9991. The drug entrapment efficiency was calculated by the following equation:

$$\text{Drug entrapment efficiency} = (\text{total PTX} - \text{free PTX})/\text{total PTX} \times 100\%$$

Measurement of streptavidin conjugated with biotinylated and PTX-loaded microbubble (BPLMBs)

The BPLMBs at a concentration of 1×10^8/ml were incubated with 0.05 μg/ml FITC-labeled streptavidin (Beijing Biosynthesis Biotechnology Co., Ltd., Beijing, China) at room temperature with a gentle shaking for 30 minutes. The incubation mixture was washed with PBS for three times to remove free FITC-labeled streptavidin and obtain the avidinylated

microbubbles labeled with FITC. The microbubbles were diluted with PBS and the fluorescence intensity was determined by a FACScan flow cytometer. The relative level of avidin bound to BPLMBs was determined by the mean fluorescence intensity of FITC in the BPLMBs. All experiments were carried out in triplicate.

Detection of LHRHa on TPLMBs' surface

The LHRHa peptide was detected by an immunofluorescent assay. Briefly, TPLMBs were blocked with goat serum for 30 minutes at room temperature and then incubated overnight with 1:100 anti-LHRH rabbit polyclonal antibodies (Biosynthesis, Beijing, China) at 4 °C. After washed with PBS (1000 g for three minutes) for three times, the MBs were incubated with 1:100 Cy3-labeled goat anti-rabbit IgG (Biosynthesis, Beijing, China) at 37°C for 30 minutes. After that, the TPLMBs were washed again with PBS (1000 g for three minutes) for three times and imaged by a TCS SP5 laser scanning confocal microscope (Leica, Wetzlar, Germany).

Measurement of LHRHa concentration on the surface of TPLMBs

The relative level of LHRHa peptides bound to TPLMBs was determined by measuring the mean fluorescence intensity of Cy3. The result was compared with that of the BPLMBs and BSPLMBs. The LHRH polyclonal antibody (CHEMICON International, Inc., Shanghai, China) was mixed with TPLMBs, BPLMBs, and biotin- streptavidin- PTX-loaded lipid MBs (BSPLMBs) respectively, incubated at 4 °C for overnight, and washed with PBS for three times to remove the free antibody. Subsequently, TPLMBs, BPLMBs and BSPLMBs were incubated in the dark with Cy3-labeled Affinipure goat Anti-Rabbit IgG at 4 °C for one hour and washed with PBS for three times. The relative levels of LHRHa peptides bound to MBs were determined by a FACScan flow cytometer. All the experiments were carried out in triplicate.

Targeted binding of TPLMBs *in vitro*

The binding affinity of the TPLMBs was tested on the LHRH receptor positive ovarian cancer cells. A2780/DDP cells (5×10^4/ml) were incubated in Costar cell culture clusters at 37°C in a humidified atmosphere of 5% CO_2 for 24 hours. After that, the TPLMBs (1×10^5/ml) and the NTPLMBs (1×10^5/ml) were added to the cell medium respectively. Considering the buoyancy of the MBs, the cell culture clusters were placed upside down to maximize the cell-MB interaction. After a 30 minute of static exposure, the clusters were washed in PBS for three times to remove the unbound MBs. The MBs bound to the cells was examined by a bright field microscope.

Ultrasound mediated delivery of PTX

A2780/DDP cells (2×10^5 cells/well) were seeded in a 6-well plate for 24 hours to allow cell adhesion. After that, the cells were equally divided into the following seven treatment groups: (a) applying PBS only (i.e., "negative control"); (b) applying PTX only (i.e., "PTX only"); (c) applying PTX followed by ultrasound mediation (i.e., "PTX+US"); (d) applying NPLMBs only (i.e., "NPLMBs only"); (e) applying NPLMBs followed by ultrasound destruction (i.e., "NPLMBs+US"); (f) applying TPLMBs only (i.e., "TPLMBs only"); (g) applying TPLMBs followed by ultrasound destruction (i.e., "TPLMBs+US"). For treatment groups (b)–(g), PTX was administered at a dose of 0.25 μg/ml. For treatment groups (c), (e), and (g), ultrasound pulses with an average intensity of 0.5 W/cm^2 were applied to the medium for 30 seconds after PTX, TPLMB or NPLMB were added to the cell medium for 30 minutes. The ultrasound transducer was a piezoelectric ceramic unfocused transducer (model UGT1025, Ultrasonographic Image Research Institute, Chongqing Medical

University, Chongqing, China) with a diameter of one centimeter and a frequency of 300 KHz, immersed 2 mm above the cell suspension within the cell culture medium.

Cell viability assay

After exposure to ultrasound pulses, the cells were seeded in a 24 well plate, incubated for 24, 48 and 72 hours and washed in PBS for three times. The number of viable cells in each treatment group relative to PBS control was assessed using a 3-(4,5-dimethylthiazol-2-yl)-2,5-diphenyltetrazolium bromide (MTT) assay.

Apoptosis assay

At 24 hours after different treatments, the cell apoptosis was evaluated by staining them with an annexin V/PI apoptosis kit (Hangzhou Longji Biological Technology Co., LTD, Hangzhou, China) following the manufacturer's instructions. Propidium iodide (PI) at a concentration of 0.5 μg/mL was added to the cell suspension immediately before flow cytometry analysis (BD Biosciences, USA).

Cell cycle analysis

24 hours after treatments, the cells were harvested with trypsin (0.05%)/EDTA (0.02%), washed twice with PBS, and fixed with 75% ethanol at 4°C for overnight, After that, the cells were incubated in 0.25 mg/ml ribonuclease solution at 37 °C for 30 minutes, followed by staining with 50 μl/ml PI on ice and in the dark for 30 minutes. For both the control and the treatment groups, the cell cycles were analyzed by a flow cytometer (BD Biosciences, USA). The percentages of the cells at G1, S, G2/M phases of the cell cycle were analyzed by a ModiFit cell cycle analysis software package (BD Biosciences, USA).

Caspase-3 and cyclinB1 activity

The Caspase-3 and cyclinB1 protein expressions of the A2780/DDP cells were characterized by Western Blot analysis. 24 hours after treatment, the cells in each group were lyzed in a lysis buffer (50 mM Tris–Cl, pH 7.4,1 mM EDTA, 150 mM NaCl, 1% nonidet P40, 0.25% Na-deoxycholate, and 1 μg/ml of aprotinin, leupeptin, and pepstatin). The protein content was quantified according to the Bradford method.[22] Equal amounts of protein (30 μg/sample) were separated electrophoretically by 12% SDS-PAGE and blotted onto a polyvinylidene difluoride (PVDF) membrane. The membranes were blocked with PBS containing 5% non-fat dried milk for at least one hour, and the blots were probed with rabbit anti-caspase-3 (1:100; Zhongshan Golden Bridge Biotechnology, Beijing, China) and rabbit anti-cyclinB1 (1:200; Santa Cruz Biotechnology Inc, Santa Cruz, California, USA) overnight at 4 °C, followed by incubation with horseradish peroxidase-conjugated anti-IgG in a blocking buffer for one hour. After washing, the blots were developed with enhanced chemiluminescence (ECL) and exposed to X-ray film (Eastman-Kodak, Rochester, NY, USA). Band optical density (OD) was analyzed using a Labworks 4.6 UVP-image capture and analysis software package. The analysis results were expressed in the format of mean ± standard deviation (SD) as the ratio percentage of the protein of interest OD versus the GAPDH OD.

Transmission electron microscopic analysis

The ultrastructural morphology of the untreated and treated A2780/DDP cells was investigated by transmission electron microscopy as described previously[23]. In brief, 24 hours after different treatments, the A2780/DDP cells were washed with PBS, trypsinized, pelleted by centrifugation (400 g) at 4°C for 15 minutes, and fixed with 2.5% glutaraldehyde. The cells were photographed by an H7500 transmission electron microscope (Hitachi Co. Ltd, Japan) following the standard protocol.

Statistical analysis

The SPSS 13.0 software package was used for data analysis. Data are expressed in the form of mean ± SD. One-way ANOVA and the Student-Newman-Keuls test were used to compare the variables among different treatment groups. *P* values of less than 0.05 were considered statistically significant.

Results

Physical characterization of TPLMBs

TPLMBs were synthesized by conjugating PTX-loaded lipid MBs with LHRHa peptide through a biotin-streptavidin-biotin linkage. The synthesized TPLMBs have a size distribution of (1.8 ± 0.2) μm, a mean zeta potential of −(9.6 ± 3.2) mV, and a drug entrapment efficiency of (73.1 ± 1.6)%. In comparison, the NPLMBs have a size distribution of (1.4 ± 0.3) μm, a mean zeta potential of − (8.5 ± 2.0) mV, and a drug entrapment efficiency of (96.5 ± 1.4)%. No significant morphological difference is observed between the TPLMBs and the NPLMBs (Figure 1).

Binding of LHRHa on TPLMBs

The conjugation of LHRHa peptides with PTX-loaded MBs was confirmed by flow cytometry, immunofluorescence assay, and bright field microscopic imaging (Figure 2). Figure 2 a shows the fluorescence intensities acquired by a FACScan flow cytometer for the BPLMBs after incubation with FITC-labeled streptavidin (sample) and for the PLMBs without FITC labeling (blank control). Further analysis shows that about (99.12±1.45) % BPLMBs have been successfully coated with the FITC-labeled streptavidin. Successful conjugation of LHRHa with TPLMBs was also confirmed by flow cytometry. Figure 2b shows the fluorescence intensities of PLMBs (control), TPLMBs, BPLMBs, and BSPLMBs after incubation with LHRH polyclonal antibody and Cy3-labeled Affinipure goat Anti-Rabbit IgG (a second antibody for LHRH polyclonal antibody). TPLMBs show the largest shift of the fluorescence count peak, indicating the highest LHRHa binding affinities. In comparison, BPLMBs and BSPLMBs show minor shifts, indicating non-specific binding LHRHa to MBs. Further analysis shows that about (87.33 ± 2.19) % of TPLMBs have been successfully conjugated with Cy3-labeled Affinipure goat Anti-Rabbit IgG. In comparison, this figure is only about (21.35 ± 1.76) % for BSPLMBs and (19.27 ± 1.98) % for BPLMBs. The binding rate for TPLMBs is significantly higher than that of BSPLMBs and BPLMBs ($P<0.05$), indicating successful conjugation of LHRHa with PLMBs. Figure 2c shows the bright field and the confocal fluorescence microscopic images of the TPLMBs after incubation with anti-LHRH polyclonal antibody and Cy3-labeled IgG. The coincidence between the fluorescence image and the bright field image confirm the effective binding of LHRHa peptide on the lipid membrane of the TPLMBs. The result also indicates that binding LHRHa peptides to PTX-loaded MBs through biotin-avidin bridging does not change their immune competence. Figure 2 d compares the microscopic images of the A2780/DDP cells after applying TPLMBs and NPLMBs. According to the figure, NPLMBs do not bind with the cells (left), whereas TPLMBs bind with the cells well (right).

Cell viability after ultrasound exposure

The cytotoxicity profiles of different treatment options (i.e., PTX, TPLMB, and NPLMB) with and without ultrasound mediation was evaluated by a MTT assay and compared with the untreated cells (blank control). Figure 3 compares the cell proliferation inhibitory rates at 24 to 72 hours after different treatments. According to the figure, the cell proliferation inhibitory rate is less than 30% for treatment groups (b), (c), (d) and (f). In comparison, treatment group (e) yields the cell proliferation inhibitory rates of (37.2 ± 2.01) %, (51.6 ±

2.1) %, and (57.47 ± 2.85) % at 24, 48 and 72 hours after treatment, respectively. This figure changes to (41.30 ± 3.93) %, (67.76 ± 2.45) %, and (75.93 ± 2.81) % for group (g). Obviously, treatment group (g) results in significantly higher proliferation inhibitory rate than other treatment groups (P <0.05), indicating that ultrasound mediated TPLMBs destruction significantly inhibits the cell proliferation.

Cell apoptosis after ultrasound exposure

The apoptosis efficacy after ultrasound mediated delivery of TPLMBs to A2780/DDP cells was evaluated quantitatively by flow cytometry and western blot assay as shown in Figure 4. According to Figure 4A, the apoptosis efficiencies for treatment groups (a)–(g) are (2.81 ± 0.35)%, (8.84 ± 0.65)%, (11.18 ± 0.25)%, (2.87 ± 0.53) %, (14.76 ± 0.72) %, (2.89 ± 0.60) %, and (32.6 ± 0.79) %, respectively. In comparison with other treatment groups, group (g) results in a significantly higher apoptosis rate (P < 0.05), indicating the significant increase of the cell apoptosis efficiency by ultrasound mediated delivery of TPLMBs. Tumor apoptosis related protein caspase-3 expression after treatment was evaluated by western blot assay. As shown in Figure 4B, cells treated with ultrasound-mediated delivery of TPLMBs (i.e., group g) show more prominent bands than other treatment groups. The indexes of caspase-3/GAPDH ratio for treatment groups (a), (d), and (f) are less than 0.07, whereas those for treatment groups (b), (c), (e), and (g) are (0.25 ± 0.01), (0.27 ± 0.01), (0.33 ± 0.02), and (0.37 ± 0.01), respectively. Compared with other treatment groups, group (g) has the highest level of caspase-3 expression (P < 0.05), indicating that ultrasound mediated delivery of TPLMBs induces tumor cell apoptosis.

Cell cycle arrest after ultrasound exposure

The cell cycle changes after different treatment options were analyzed by flow cytometry and western blot test as shown in Figure 5. According to Figure 5A, the cell proportions in G0/G1, S, and G2/M phases are about 50%, 40% and 10%, respectively after treatment options (a), (d), and (f). For treatment group (c), the cell proportions in G0/G1, S, and G2/M phases are (45.90 ± 0.919)%, (24.31 ± 0.803)% and (29.78 ± 0.854)%, respectively, showing slightly increased G0/G1 and G2/M phases and slightly decreased S phases (P<0.05). These figures for treatment group (e) are (4.25 ± 0.949) %, (18.48 ± 1.046)%, and (77.27 ± 1.172)%, respectively. The cell proliferation rates in G0/G1 and G2/M phases are moderately increased and S phases are moderately decreased compared with the control group (P < 0.05). For treatment group (g), these figures become (1.39 ± 0.745)%, (8.14 ± 0.937)%, and (90.48 ± 0.941)%, respectively. The increased G0/G1 and G2/M phases and decreased S phases indicate that ultrasound mediated delivery of TPLMBs induces a significant G1 phase arrest and a concomitant reduction in the cell fraction in the S phase.

The cell cycle regulatory protein cyclin B1 was also evaluated by a western blot test. As shown in Figure 5B, cells treated with ultrasound-mediated delivery of TPLMBs (i.e., group g) shows more prominent bands than other treatment groups. The indexes of cyclin B1/GAPDH ratio for treatment groups (a), (d), and (f) are less than 0.05, whereas those for treatment groups (b), (c), (e), and (g) are (0.26 ± 0.008), (0.27 ± 0.011), (0.76 ± 0.015), and (0.93 ± 0.009), respectively. Compared with other treatment groups, group (g) has the highest level of cyclin B1 expression (P < 0.05), indicating that ultrasound mediated delivery of TPLMBs induces tumor apoptosis.

Cell morphology change after ultrasound exposure

The ultrastructural morphology of the A2780/DDP cells after ultrasound mediated delivery of TPLMBs was examined by Transmission Electron Microscopy (TEM). Figure 6 shows representative TEM images 24 hours after different treatments. According to Figure 6b, applying PTX results in more microfilaments and microtubules in the cell cytoplasm. In the

case of no ultrasound exposure, applying TPLMBs and NPLMBs does not yield obvious changes in cell morphology (Figures 6d and 6f). In comparison, with ultrasound exposure, applying PTX results in mitotic cells (Figure 6e); applying NPLMBs results in multinucleated cells (Figure 6f), and applying TPLMBs results in apoptotic cells (Figure 6g). The apoptotic cells are smaller, with concentrated cytoplasm, irregular nucleus, and highly condensed and marginalized chromatin.

DISCUSSION

Ultrasound targeted microbubble destruction (UTMD) technique is a promising approach for image guided therapy and controlled drug delivery.[24–26] Recent advances in microfabrication and molecular science have enabled the conjugation of disease targeting antibodies and peptides with MBs to enhance the binding affinity with tumor cells.[27–30] LHRH is a peptide that specifically binds to LHRH receptors overexpressed on the extracellular membrane of many ovarian tumor cells.[31] Therefore, it may serve as an ideal targeting moiety for ovarian cancer active drug delivery.[32, 33] Paclitaxel is one of the most effective chemotherapeutic drugs for the treatment of various cancers, including ovarian cancer, breast cancer, non-small cell lung cancer, and head and neck carcinomas.[34–37] Unfortunately, its clinical use in systemic therapy is limited by its poor water solubility and the lack of selective cytotoxicity between cancer cells and normal cells. Therefore, developing a disease-targeting drug therapeutic system with improved efficacy and safety is necessary. We hypothesize that UTMD of LHRHa-coated and PXT-loaded MBs will facilitate drug deposition at the tumor site for the enhanced therapeutic outcome. This hypothesis has been tested through our *in vitro* and *in vivo* experiments.

In this study, PXT-loaded targeted MBs (TPLMBs) were synthesized by conjugating a modified LHRHa peptide to the shell of PXT-loaded MBs via avidin-biotin interactions. Although this binding strategy has been demonstrated successfully in animal models, its clinical feasibility is limited by the unwanted immunogenicity. This limitation may be overcome by designing avidin in less immunogenic forms or using other covalent and non-covalent binding strategies. The TPLMBs were able to achieve a drug encapsulation efficiency of 73%, similar to that reported by other researchers.[38] The conjugation of LHRHa to the shell of PXT-loaded MBs significantly increased their adhesion to ovarian cancer A2780/DDP cells. After applying ultrasound pulses to the co-culture of A2780/DDP cells and TPLMBs, the cell proliferation inhibitory rate was significantly increased. In our study, ultrasound pulses of 300 KHz were applied to the cell at an average power intensity of 0.5 W/cm^2 for the duration of 30 seconds. Applying this level of ultrasound pulses alone may not induce a significant proliferation inhibitory effect, as evidenced by the previous study that showed no suppression of cell viability after applying ultrasound pulses of 240 kHz at an intensity of 5.76W/cm^2 for 30s.[39.40] Cell cycle analysis carried out 24 hours after treatment also revealed an induced G0/G1 phase arrest, a reduced cell fraction in S phase, an increased cell fraction in G2/M phase, and an up-regulated cycle regulatory protein cyclin B1 expression which is consistent with the previous research.[41] The mechanism behind ultrasound mediated delivery of drug-loaded MBs has not been fully understood yet. We believe that this mechanism is associated with at least the following contributing factors. First of all, the physical interaction between LHRHa peptides and LHRH receptors facilitates the adhesion of the TPLMBs on the surface of cells, shortens the distance between bioactive drugs and cancer cells, increases the local drug concentration, and reduces the time for drug delivery into cells.[19] Second, ultrasound mediation causes MB oscillation and destruction for the enhanced delivery and release of the encapsulated therapeutics.[42, 43] Third, ultrasound exposure of the MBs generates a critical transmembrane shear force lead for the increased permeability of the extracellular drugs to the cell membrane.[44] Forth, TPLMBs closed to the cancer cells are benefited from sonoporation and the enhanced drug

uptake by the cells can be achieved upon pore formation. Finally, the induction of ultrasound and MBs may increase the intracellular hydrogen peroxide (H_2O_2) level and the influx of calcium ions in cells that are directly responsible for the increased apoptosis.[45] As evidenced by our *in vitro* studies, TPLMBs plus ultrasound results in significantly higher apoptosis efficiency than other treatment groups. The cell morphology also revealed an apoptosis effect of bursting the LHRHa-targeted and Paclitaxel- loaded microbubbles with ultrasound to A2780/DDP cells.

It is reported that cytochrome c release and cleavage of caspases are involved in paclitaxel induced apoptotic.[46–49] Our experiments showed that compared with free paclitaxel, paclitaxel plus ultrasound slightly increased the caspases-3 expression. There is no significant difference in the NPLMBs and the TPLMBs groups compared with the control group, which indicated the stability of MBs. Significant increase of caspases-3 expression in A2780/DDP cells were found after TPLMBs were combined with ultrasound. MBs oscillations and the loaded drug completely release into the tumor cells can explain the mechanism of these effects.[42, 43]

In summary, we synthesized the targeted and drug loaded microbubbles for ultrasound mediated delivery of paclitaxel to ovarian cancer cells. Our study revealed that, ultrasound mediated targeted and drug loaded microbubbles destruction can accomplish a selective cytotoxicity and apoptosis effect on A2780/DDP cells in vitro. Our *in vivo* study in an ovarian cancer xenograft model also demonstrated the anticancer effect after ultrasound mediated delivery of cancer-targeted and drug-loaded microbubbles.[50] The TPLMBs mediated by ultrasound may present a novel and attractive approach for ovarian cancer

Acknowledgments

The authors are grateful to Dr. Pan Li (Institute of Ultrasound Imaging, Second Hospital of Chongqing Medical University, and Chongqing, China) for the helpful technical discussion, Dr. Zehua Wang (Department of Obstetrics and Gynecology, Tongji Medical College, Wuhan Union hospital Huazhong University of Science and Technology, Wuhan, China) for the kind supply of A2780/DDP cells, Dr. Ting Si (University of Science and Technology of China, Hefei, China) for the helpful illustration editing and Dr. Zhibiao Wang (Director of National Engineering Research Center of Ultrasound Medicine, Chongqing Medical University, Chongqing, China) for the generous support of the experimental facilities. This research was supported by Natural Science Foundation of China (81372799), Bureau of Health Foundation of Chongqing (2010-1-6, 2010-1-39) and National High Technology Research and Development Program of China (2006AA02Z4FO)), and National Cancer Institute (R21CA15977).

Abbreviations Used

MBs	microbubbles
US	ultrasound
UTMD	ultrasound-targeted microbubble destruction
PTX	paclitaxel
TPLMBs	LHRH receptor targeted and paclitaxel loaded lipid microbubbles
NPLMBs	non-target PTX-loaded microbubbles
LHRH-R	luteinizing hormone-releasing hormone receptor
LHRHa	LHRH analogue
TEM	transmission electron microscopy
PBS	phosphate buffered saline
PLMBs	PTX-loaded MBs

BPLMBs	biotin-paclitaxel loaded microbubble
BSPLMBs	biotin-streptavidin-PTX loaded lipid microbubbles
MTT	3-(4,5-dimethylthiazol-2-yl)-2,5-diphenyltetrazolium bromide
PVDF	polyvinylidene difluoride

References

1. Desantis C, Naishadham D, Jemal A. Cancer statistics for African Americans, 2013. CA Cancer J Clin. 2013; 63(3):151–166. [PubMed: 23386565]
2. Maringe C, Walters S, Butler J, Coleman MP, Hacker N, Hanna L, Mosgaard BJ, Nordin A, Rosen B, Engholm G, Gjerstorff ML, Hatcher J, Johannesen TB, McGahan CE, Meechan D, Middleton R, Tracey E, Turner D, Richards MA, Rachet B. Stage at diagnosis and ovarian cancer survival: evidence from the International Cancer Benchmarking Partnership. Gynecol Oncol. 2012; 127(1): 75–82. [PubMed: 22750127]
3. Assis J, Pereira D, Gomes M, Marques D, Marques I, Nogueira A, Catarino R, Medeiros R. Influence of CYP3A4 genotyped in the outcome of serous ovarian cancer patients treated with first-line chemotherapy:implication of a CYP3A4 activity profile. Clin Exp Med. 2013; 6(7):552–561.
4. Doi D, Ota Y, Konishi H, Yoneyama K, Araki T. Evaluation of the neurotoxicity of paclitaxel and carboplatin by current perception threshold in ovarian cancer patients. J Nippon Med Sch. 2003; 70(2):129–134. [PubMed: 12802373]
5. Doyle T, Chen Z, Muscoli C, Bryant L, Esposito E, Cuzzocrea S, Dagostino C, Ryerse J, Rausaria S, Kamadulski A, Neumann WL, Salvemini D. Targeting the overproduction of peroxynitrite for the prevention and reversal of paclitaxel-induced neuropathic pain. J Neurosci. 2012; 32(18):6149–6160. [PubMed: 22553021]
6. Pachman DR, Barton DL, Watson JC, Loprinzi CL. Chemotherapy-induced peripheral neuropathy: prevention and treatment. Clin Pharmacol Ther. 2011; 90(3):377–387. [PubMed: 21814197]
7. Gupta YK, Sharma SS, Rai K, Katiyar CK. Reversal of paclitaxel induced neutropenia by Withania somnifera in mice. Indian J Physiol Pharmacol. 2001; 45(2):253–257. [PubMed: 11480235]
8. Mura S, Couvreur P. Nanotheranostics for personalized medicine. Adv Drug Deliv Rev. 2013; 64(13):1394–416. [PubMed: 22728642]
9. Allen TM, Cullis PR. Liposomal drug delivery systems: from concept to clinical applications. Adv Drug Deliv Rev. 2013; 65(1):36–48. [PubMed: 23036225]
10. Geis NA, Katus HA, Bekeredjian R. Microbubbles as a vehicle for gene and drug delivery: current clinical implications and future perspectives. Curr Pharm Des. 2012; 18(15):2166–2183. [PubMed: 22352771]
11. Escoffre JM, Zeghimi A, Novell A, Bouakaz A. In-vivo gene delivery by sonoporation: recent progress and prospects. Curr Gene Ther. 2013; 3(1):2–14. [PubMed: 23157546]
12. Hamano N, Negishi Y, Omata D, Takahashi Y, Manandhar M, Suzuki R, Maruyama K, Nomizu M, Aramaki Y. Bubble liposomes and ultrasound enhance the antitumor effects of AG73 liposomes encapsulating antitumor agents. Mol Pharm. 2013; 10(2):774–779. [PubMed: 23210449]
13. Florinas S, Nam HY, Kim SW. Enhanced siRNA delivery using a combination of an arginine-grafted bioreducible polymer, ultrasound and microbubbles in cancer cells. Mol Pharm. 2013; 10(5):2021–2030. [PubMed: 23527953]
14. Escoffre JM, Piron J, Novell A, Bouakaz A. Doxorubicin delivery into tumor cells with ultrasound and microbubbles. Mol Pharm. 2011; 8(3):799–806. [PubMed: 21495672]
15. Xing W, Gang WZ, Yong Z, Yi ZY, Shan XC, Tao RH. Treatment of xenografted ovarian carcinoma using paclitaxel-loaded ultrasound microbubbles. Acad Radiol. 2008; 15(12):1574–1579. [PubMed: 19000874]

16. Cochran MC, Eisenbrey J, Ouma RO, Soulen M, Wheatley MA. Doxorubicin and paclitaxel loaded microbubbles for ultrasound triggered drug delivery. Int J Pharm. 2011; 414(1–2):161–170. [PubMed: 21609756]

17. Rapoport NY, Kennedy AM, Shea JE, Scaife CL, Nam KH. Controlled and targeted tumor chemotherapy by ultrasound-activated nanoemulsions/microbubbles. J Control Releas. 2009; 138(3):268–276.

18. Tartis MS, McCallan J, Lum AF, LaBell R, Stieger SM, Matsunaga TO, Ferrara KW. Therapeutic effects of paclitaxel-containing ultrasound contrast agents. Ultrasound Med Biol. 2006; 32(11): 1771–1780. [PubMed: 17112963]

19. Yan F, Li X, Jin Q, Jiang C, Zhang Z, Ling T, Qiu B, Zheng H. Therapeutic ultrasonic microbubbles carrying paclitaxel and LyP-1 peptide: preparation, characterization and application to ultrasound-assisted chemotherapy in breast cancer cells. Ultrasound Med Biol. 2011; 37(5): 768–779. [PubMed: 21458148]

20. Chang S, Guo J, Sun J, Zhu S, Yan Y, Zhu Y, Li M, Wang Z, Xu RX. Targeted microbubbles for ultrasound mediated gene transfection and apoptosis induction in ovarian cancer cells. Ultrason Sonochem. 2012; 20(1):171–179. [PubMed: 22841613]

21. Kang J, Wu X, Wang Z, Ran H, Xu C, Wu J, Wang Z, Zhang Y. Antitumor effect of docetaxel-loaded lipid microbubbles combined with ultrasound-targeted microbubble activation on VX2 rabbit liver tumors. J Ultrasound Med. 2010; 29(1):61–70. [PubMed: 20040776]

22. Bradford MM. Rapid and sensitive method for quantitation of microgram quantities of protein utilizing principle of protein-dye binding. Analytical Biochemistry. 1976; 72(1–2):248–254. [PubMed: 942051]

23. Gao X, Zhang Y, Chen H, Chen Z, Lin X. Amperometric immunosensor for carcinoembryonic antigen detection with carbon nanotube-based film decorated with gold nanoclusters. Analytical Biochemistry. 2011; 414(1):70–76. [PubMed: 21396907]

24. Escoffre JM, Mannaris C, Geers B, Novell A, Lentacker I, Averkiou M, Bouakaz A. Doxorubicin liposome-loaded microbubbles for contrast imaging and ultrasound-triggered drug delivery. IEEE Trans Ultrason Ferroelectr Freq Control. 2013; 60(1):78–87. [PubMed: 23287915]

25. Li P, Zheng Y, Ran H, Tan J, Lin Y, Zhang Q, Ren J, Wang Z. Ultrasound triggered drug release from 10-hydroxycamptothecin-loaded phospholipid microbubbles for targeted tumor therapy in mice. J Control Release. 2012; 162(2):349–354. [PubMed: 22800580]

26. Liao AH, Li YK, Lee WJ, Wu MF, Liu HL, Kuo ML. Estimating the delivery efficiency of drug-loaded microbubbles in cancer cells with ultrasound and bioluminescence imaging. Ultrasound Med Biol. 2012; 38(11):1938–1948. [PubMed: 22929655]

27. Xu JS, Huang J, Qin R, Hinkle GH, Povoski SP, Martin EW, Xu RX. Synthesizing and binding dual-mode poly (lactic-co-glycolic acid) (PLGA) nanobubbles for cancer targeting and imaging. Biomaterials. 2009; 31(7):1716–1722. [PubMed: 20006382]

28. Xu RX, Povoski SP, Martin EW Jr. Targeted delivery of microbubbles and nanobubbles for image-guided thermal ablation therapy of tumors. Expert Rev Med Devices. 2009; 7(3):303–306. [PubMed: 20420552]

29. Anderson CR, Rychak JJ, Backer M, Backer J, Ley K, Klibanov AL. scVEGF microbubble ultrasound contrast agents: a novel probe for ultrasound molecular imaging of tumor angiogenesis. Invest Radiol. 2010; 45(10):579–585. [PubMed: 20733505]

30. Patel RM. Microbubble: a potential ultrasound tool in molecular imaging. Curr Pharm Biotechnol. 2008; 9(5):406–410. [PubMed: 18855694]

31. Volker P, Grundker C, Schmidt O, Schulz KD, Emons G. Expression of receptors for luteinizing hormone-releasing hormone in human ovarian and endometrial cancers: frequency, autoregulation, and correlation with direct antiproliferative activity of luteinizing hormone-releasing hormone analogues. Am J Obstet Gynecol. 2002; 186(2):171–179. [PubMed: 11854630]

32. Dharap SS, Qiu B, Williams GC, Sinko P, Stein S, Minko T. Molecular targeting of drug delivery systems to ovarian cancer by BH3 and LHRH peptides. J Control Release. 2003; 91(1–2):61–73. [PubMed: 12932638]

33. Kim SH, Jeong JH, Lee SH, Kim SW, Park TG. LHRH receptor-mediated delivery of siRNA using polyelectrolyte complex micelles self-assembled from siRNA-PEG-LHRH conjugate and PEI. Bioconjug Chem. 2008; 19(11):2156–2162. [PubMed: 18850733]
34. Hu Q, Li W, Hu X, Shen J, Jin X, Zhou J, Tang G, Chu PK. Synergistic treatment of ovarian cancer by co-delivery of survivin shRNA and paclitaxel via supramolecular micellar assembly. Biomaterials. 2012; 33(27):6580–6591. [PubMed: 22717365]
35. Hong RL, Lin CH, Chao TY, Kao WY, Wang CH, Hsieh RK, Hwang WS. A phase-I study evaluating the combination of pegylated liposomal doxorubicin and paclitaxel as salvage chemotherapy in metastatic breast cancer previously treated with anthracycline. Cancer Chemother Pharmacol. 2008; 61(5):847–853. [PubMed: 17609947]
36. Kaplan B, Altynbas M, Eroglu C, Karahacioglu E, Er O, Ozkan M, Bilgin M, Canoz O, Gulmez I, Gulec M. Preliminary results of a phase II study of weekly paclitaxel (PTX) and carboplatin (CBDCA) administered concurrently with thoracic radiation therapy (TRT) followed by consolidation chemotherapy with PTX/CBDCA for stage III unresectable non-small-cell lung cancer (NSCLC). Am J Clin Oncol. 2004; 27(6):603–610. [PubMed: 15577439]
37. Yared JA, Tkaczuk KH. Update on taxane development: new analogs and new formulations. Drug Des Devel Ther. 2012; 6:371–384.
38. Yan F, Li X, Jin Q, Jiang C, Zhang Z, Ling T, Qiu B, Zheng H. Therapeutic ultrasonic microbubbles carrying paclitaxel and LyP-1 peptide: preparation, characterization and application to ultrasound-assisted chemotherapy in breast cancer cells. Ultrasound Med Biol. 2011; 37(5): 768–779. [PubMed: 21458148]
39. Yu T, Hu K, Bai J, Wang Z. Reversal of adriamycin resistance in ovarian carcinoma cell line by combination of verapamil and low-level ultrasound. Ultrason Sonochem. 2003; 10(1):37–40. [PubMed: 12457949]
40. Yu T, Bai J, Hu K, Wang Z. Biological effects of ultrasound exposure on adriamycin-resistant and cisplatin-resistant human ovarian carcinoma cell lines in vitro. Ultrason Sonochem. 2004; 11(2): 89–94. [PubMed: 15030785]
41. Gomez LA, de Las Pozas A, Reiner T, Burnstein K, Perez-Stable C. Increased expression of cyclin B1 sensitizes prostate cancer cells to apoptosis induced by chemotherapy. Mol Cancer Ther. 2007; 6(5):1534–1543. [PubMed: 17513602]
42. Luan Y, Faez T, Gelderblom E, Skachkov I, Geers B, Lentacker I, van der Steen T, Versluis M, de Jong N. Acoustical properties of individual liposome-loaded microbubbles. Ultrasound Med Biol. 2012; 38(12):2174–2185. [PubMed: 23196203]
43. Escoffre JM, Novell A, Piron J, Zeghimi A, Doinikov A, Bouakaz A. Microbubble attenuation and destruction: are they involved in sonoporation efficiency? IEEE Trans Ultrason Ferroelectr Freq Control. 2013; 60(1):46–52. [PubMed: 23287912]
44. Geers B, Lentacker I, Alonso A, Sanders NN, Demeester J, Meairs S, De Smedt SC. Elucidating the mechanisms behind sonoporation with adeno-associated virus-loaded microbubbles. Mol Pharm. 2011; 8(6):2244–2251. [PubMed: 22014166]
45. Juffermans LJ, Meijering DB, van Wamel A, Henning RH, Kooiman K, Emmer M, de Jong N, van Gilst WH, Musters R, Paulus WJ, van Rossum AC, Deelman LE, Kamp O. Ultrasound and microbubble-targeted delivery of therapeutic compounds: ICIN Report Project 49: Drug and gene delivery through ultrasound and microbubbles. Neth Heart J. 2009; 17(2):82–86. [PubMed: 19247472]
46. Morales-Cano D, Calvino E, Rubio V, Herraez ASancho P, Tejedor MC, Diez JC. Apoptosis induced by paclitaxel via Bcl-2, Bax and caspases 3 and 9 activation in NB4 human leukaemia cells is not modulated by ERK inhibition. Exp Toxicol Pathol. 2013 (in press) S0940-2993(13)00058-4 [pii]. 10.1016/j.etp.2013.04.006
47. von Haefen C, Wieder T, Essmann F, Schulze-Osthoff K, Dorken B, Daniel PT. Paclitaxel-induced apoptosis in BJAB cells proceeds via a death receptor-independent, caspases-3/-8-driven mitochondrial amplification loop. Oncogene. 2003; 22(15):2236–2247. [PubMed: 12700660]
48. Selimovic D, Hassan M, Haikel Y, Hengge UR. Taxol-induced mitochondrial stress in melanoma cells is mediated by activation of c-Jun N-terminal kinase (JNK) and p38 pathways via uncoupling protein 2. Cell Signal. 2008; 20(2):311–322. [PubMed: 18068334]

49. Son YO, Choi KC, Lee JC, Kook SH, Lee SK, Takada K, Jang YS. Involvement of caspase activation and mitochondrial stress in taxol-induced apoptosis of Epstein-Barr virus-infected Akata cells. Biochim Biophys Acta. 2006; 1760(12):1894–1902. [PubMed: 16938399]

50. Pu C, Chang S, Sun J, Liu H, Zhu S, Zhu Y, Wang Z, Xu RX. Treatment of intraperitoneal ovarian cancer xenografts by ultrasound mediated delivery of tumor-specific paclitaxel-loaded microbubbles. Molecular Pharmaceutics. 2013 submitted.

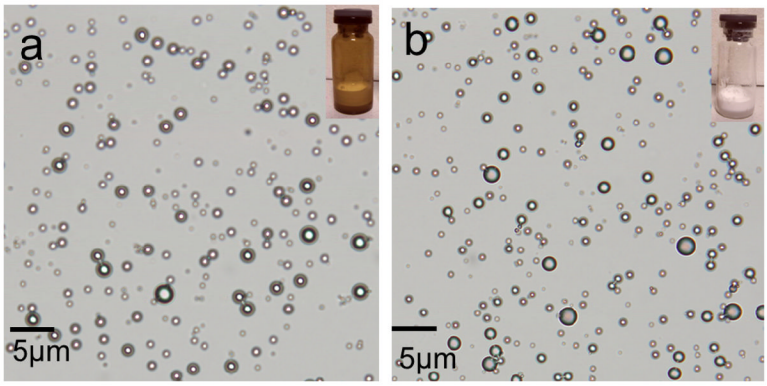

Figure 1.

Microscopic images of: (a) non-targeted paclitaxel lipid microbubbles (NPLMBs), (b) LHRH-targeted paclitaxel lipid microbubbles (TPLMBs). The insets at the upper right corner are photographs of the microbubbles. No morphologic difference is observed between NPLMBs and TPLMBs.

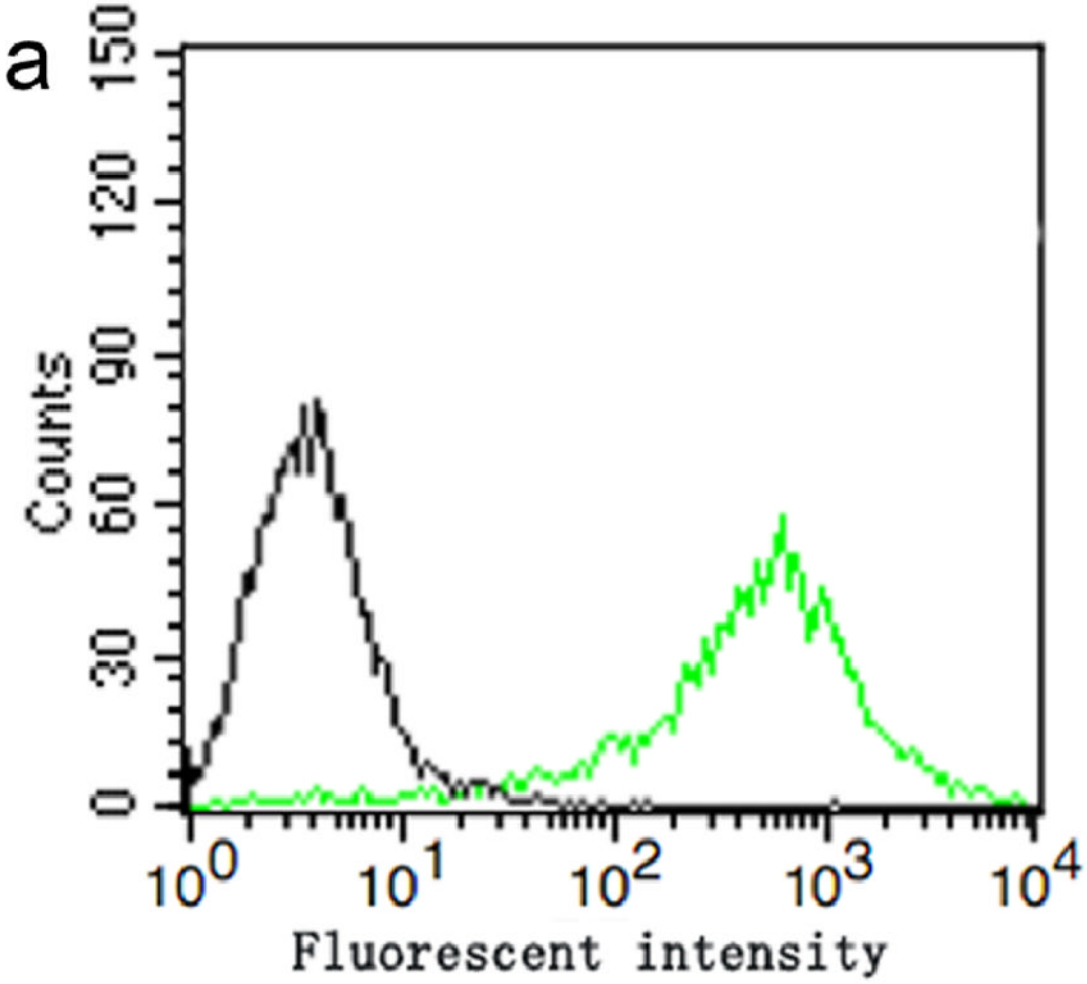

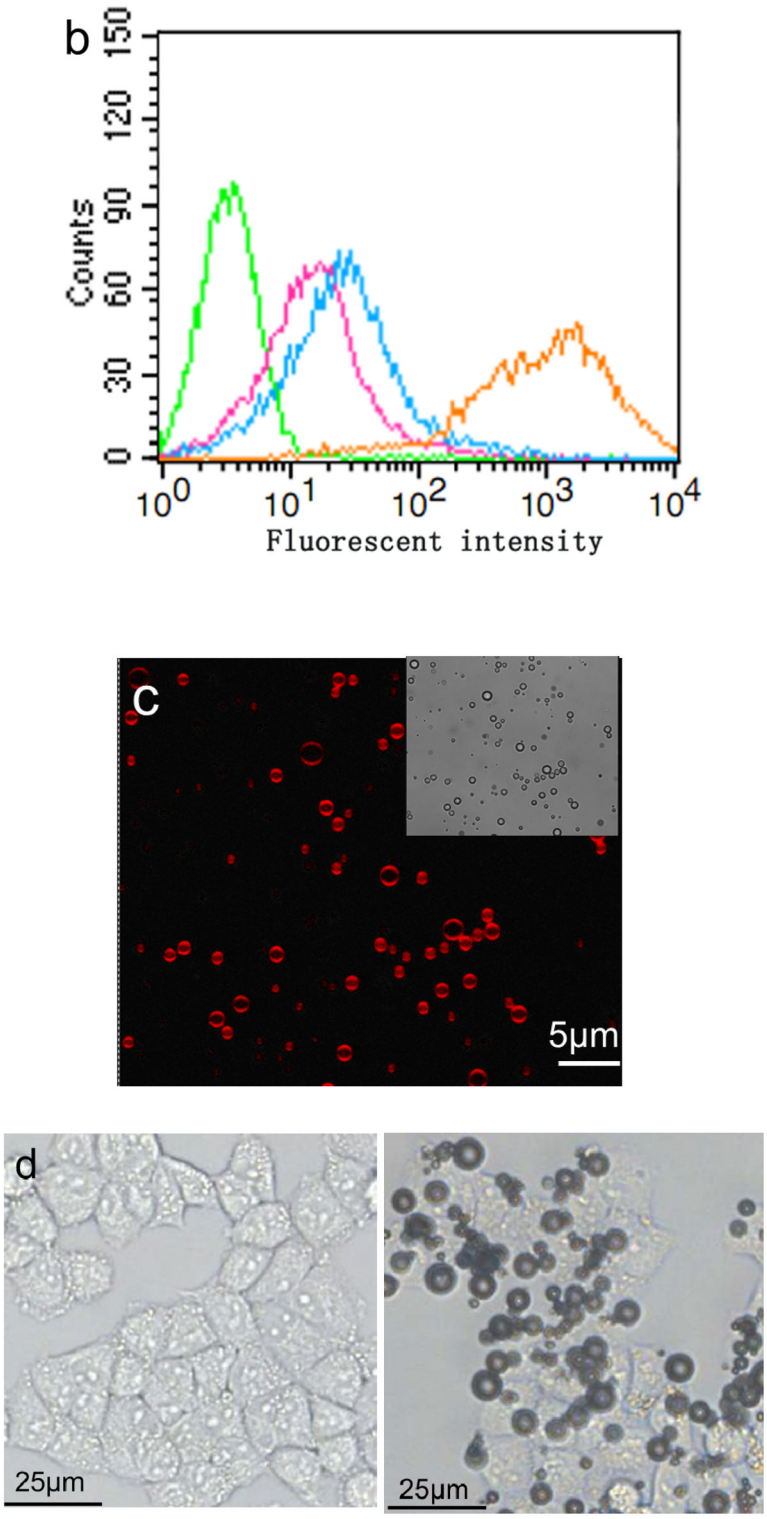

Figure 2.

In vitro analysis of PTX-loaded and LHRHa targeted MBs (TPLMBs) (a) Binding efficiency of BPLMBs with FITC-labeled streptavidin was determined by flow cytometry. Comparison of the fluorescence intensities for PLMBs (black line, control) and FITC-labeled BPLMBs

(green line) implies successful binding of FITC-labeled streptavidin with PLMBs. (b) Fluorescent intensities acquired by flow cytometry for different types of microbubbles after incubation with LHRH polyclonal antibody and Cy3 labeled IgG. Green line (blank control): PLMBs without conjugation of LHRHa. Pink line: Cy3-labeled BPLMBs. Blue line: Cy3 - labeled BSPLMBs. Orange line: Cy3 –labeled TPLMBs. (c) LHRHa peptide on TPLMBs was observed by laser scanning confocal microscope. TPLMBs were incubated with LHRH polyclonal antibody and Cy3 labeled IgG. (d) Microscopic images of A2780/DDP cells after: incubation with PLMBs (left), incubation with TPLMBs (right). The cells were washed by PBS three times before imaging. In comparison with paclitaxel loaded lipid microbubbles (PLMBs), LHRHa-targeted paclitaxel lipid microbubbles (TPLMBs) bind well with A2780/DDP cells.

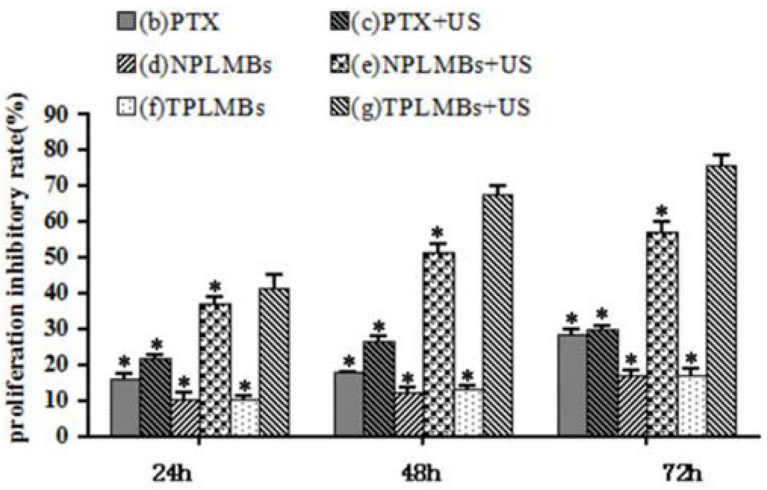

Figure 3.

Growth inhibition effect of A2780/DDP cells with different treatments. The proliferation inhibitory rate of cells was determined by MTT 24,48 and 72h after treatment. Data are represented as mean ± SD (n=3). The proliferation inhibitory rate of the PLMBs +US groups and TPLMBs +US groups are significantly higher than those of the other groups ($p<0.05$). The proliferation inhibitory rate of TPLMBs +US group is higher than PLMBs +US group at 24, 48 and 72h after treatment ($p<0.05$). Compared with group (g), *$p<0.05$.

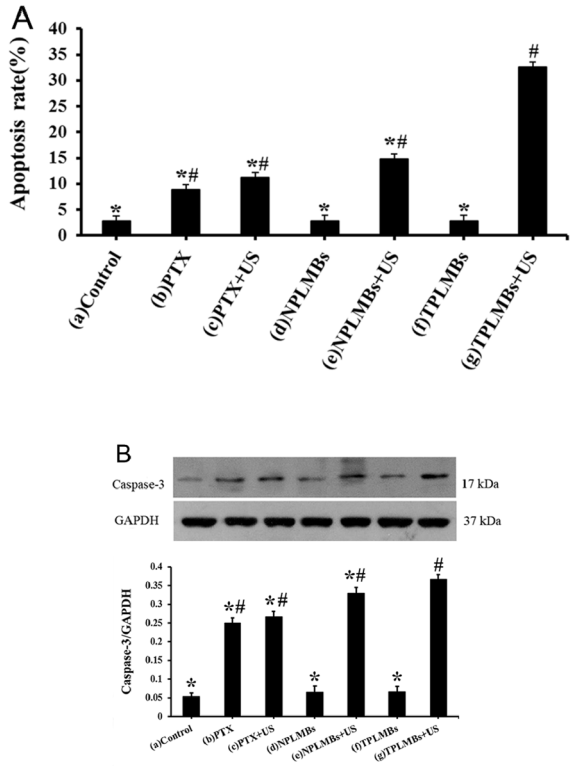

Figure 4.

Apoptosis efficiency in A2780/DDP cells with different treatments. (A) The percentage of apoptosis cells was determined by flow cytometry 24 h after transfection. Data are represented as mean ±SD (n=3). Apoptosis efficiency of the PLMBs +US groups and TPLMBs +US groups are significantly higher than those of the other groups ($P<0.05$). Apoptosis efficiency of TPLMBs +US group is higher than PLM+US group ($P<0.05$). Compared with group (g), $P<0.05$; Compared with group (a), #$P<0.05$. (B) Western blot analysis of the expression of Caspase-3 protein in A2780/DDP cells after different treatments. Caspase-3 protein expression was analyzed by Western blot 24 h after transfection. Cells treated with TPLMBs +US groups showed more prominent bands than other treatment groups ($p<0.05$). GAPDH was used as an internal reference. Compared with group (g), *$p<0.05$; Compared with group (a), #$p<0.05$.

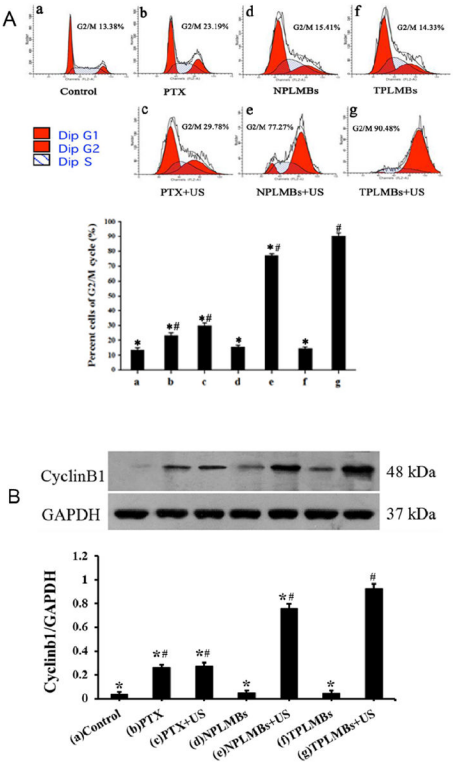

Figure 5.

The cell cycle arrest in A2780/DDP cells with different treatments. (A) Cell cycles were detected by flow cytometry 24 h after treatment. G2/M phase is significantly increased and S phase is decreased in PLMBs +US group and TPLMBs +US group than the other groups ($p < 0.05$). G2/M phase is of TPLMBs +US group is higher than PLMBs +US group and S phase is lower than PLMBs +US group ($p<0.05$). (B) Western blot analysis of the expression of cyclinB1 protein in A2780/DDP cells after different treatments. CyclinB1 protein expression was analyzed by Western blot 24 h after transfection. Cells treated with ultrasound-targeted PLMT destruction showed more prominent bands than other treatment groups ($P<0.05$). GAPDH was used as an internal reference. Compared with group (g), *$P<0.05$; Compared with group (a), #$P<0.05$.

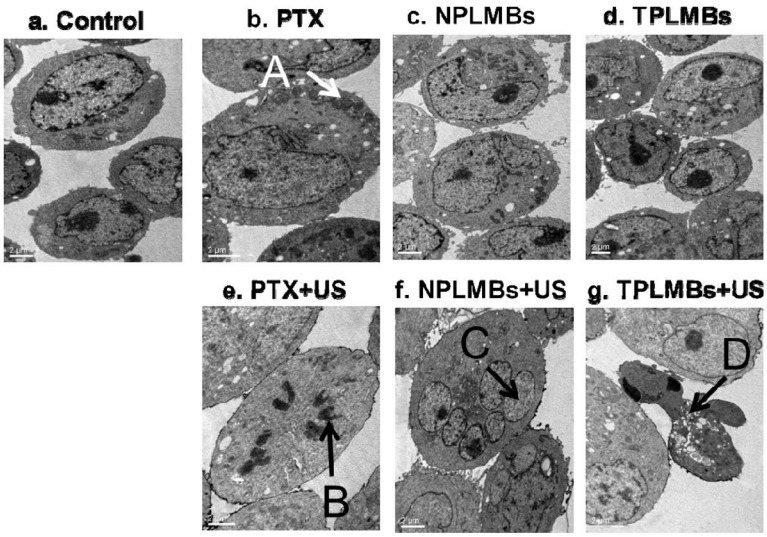

Figure 6.

Ultrastructural morphologies of A2780/DDP cells observed under TEM at 24 hour after different treatments: (a) no treatment (“control”), (b) applying PTX only (“PTX”), (c) applying NPLMBs only (“NPLMBs”), (d) applying TPLMBs only (“TPLMBs”), (e) ultrasound mediated delivery of PTX (“PTX+US”), (f) ultrasound mediated delivery of NPLMBs (“NPLMBs+US”), and (g) ultrasound mediated delivery of TPLMBs (“TPLMBs +US”). A: microfilaments and microtubes; B: mitotic cells; C: nucleus; D: apoptosis body. Scale bar is 2μm.